Type Synthesis of 5-DOF Redundantly Actuated Parallel Mechanisms for Super-Large Components

Bing-Shan Jiang (17116381@bjtu.edu.cn)
Beijing Jiaotong University
Hai-Rong Fang
Beijing Jiaotong University
Yue-Fa Fang
Staffordshire University
Li-Tao He
Beijing Jiaotong University

Original Article

Keywords: Redundantly actuated parallel mechanism, Type synthesis, Articulated moving platform, Motion simulation, Trajectory planning, Quadratic function-cosine curve

Posted Date: October 25th, 2021

DOI: https://doi.org/10.21203/rs.3.rs-987944/v1

Type synthesis of 5-DOF redundantly actuated parallel mechanisms for super-large components

Bing-Shan Jiang[1]• Hai-Rong Fang[1] • Yue-Fa Fang[1] • Li-Tao He[1]

Received June xx, 202x; revised February xx, 202x; accepted March xx, 202x

Abstract: Super-large components with complicated surfaces are used for many applications, the processing method of super-large components with complicated surfaces is also problem to be solved. The 5-edgrees of freedom (DOF) redundantly actuated parallel mechanisms (RAPMs) can be used as a movable parallel module in a multi-axis machine center to process super-large components with complicated surfaces. This paper focuses on type synthesis of 5-DOF RAPMs redundantly actuated parallel mechanisms for Super-large components. First, two articulated moving platform and four kinds of limbs are designed based on configuration evolution and Li group theory. By means of the proposed articulated moving platforms and four kinds of limbs, a series of 3T2Rand 2T3R are synthesized. Then, kinematics of the proposed RAPM is analyzed. To ensure the proposed RAPM without impact, a new trajectory planning method combining quadratic function with cosine is proposed and applied to motion simulation. The results show the RAPM not only possesses large output rotational angles, but also verifies the efficiency of the trajectory planning method in motion simulation. The work lays the foundation for solving the processing method of super-large components with complicated surfaces.

Keywords: Redundantly actuated parallel mechanism • Type synthesis • Articulated moving platform • Motion simulation • Trajectory planning • Quadratic function-cosine curve

1 Introduction

With the development of science and technology, super-large components with complicated surfaces is used for many applications, and the processing method of super-large components with complicated surfaces is also problem to be solved. The requirements for the quality and performance of the components are also increasing. However, super-large components with complicated surfaces have characteristics of enormous size, small-batch, difficult to move. It is difficult to machine super-large components with complicated surfaces. Redesigning a 1:1 special machine tool is not in line with the development trend. Therefore, it is necessary to redesign the processing robot for super-large components with complicated surfaces. The processing robot not only meets variable size super-large components, but also meets the processing of local complicated surfaces. For the processing requirements of oversized components [1–3], the components are divided into many areas, which can be processed by the 5-DOF parallel module, and then the whole area of oversized components can be processed by the removable robot. For the processing requirements of components with complicated surfaces [4–6], [11], the components are processed by the 5-axis machine center. Compared with the serial module in the 5-axis machine center, the parallel module has the advantages of high rigidity, high accuracy, and good dynamic performance [7–9] in the 5-axis machine center. To solve the processing of super-large components with complicated surfaces, this paper presents 8-axis five linkage hybrid removable robot, which contains a 5-DOF parallel module and three orthogonal long rails, as shown in Figure 1. The 5-DOF parallel module in Figure 1 is enlarged in Figure 2. The super-large component with complex surface is divided into N areas, as shown in Figure 3. The operating principle of 8-axis five linkage hybrid removable robot machining super-large components with complicated surfaces is that the three orthogonal long rails will move the 5-DOF parallel module to the region 1, and then the 5-DOF parallel module independently processes the region 1. When the 5-DOF parallel module finishes the region 1, then the three orthogonal long rails will move the 5-DOF parallel module to the region 2, and the 5-DOF parallel module independently processes the region 2, and so on. Three orthogonal long rails only have positioning function, and the 5-DOF parallel module processes local complicated surfaces, independently. To ensure the machining accuracy of super-large components with complicated surfaces, the 8-axis five linkage hybrid removable robot should move smoothly and have no vibration impact. However, the super-large component with complicated surfaces also contains some convex-concave structures. The 5-DOF parallel module with large output rotational angles is helpful to process the convex-concave structures of super-large components. However, the mechanical body of the 5-DOF parallel module is a 5-DOF parallel mechanism. This paper focuses on type synthesis of 5-DOF RAPMs with large output rotational angles to process local complicated surfaces of the super-large components.

✉ Hai-Rong Fang
hrfang@bjtu.edu.cn
[1] Robotics Research Center, Beijing Jiao Tong University, Beijing 10044, China

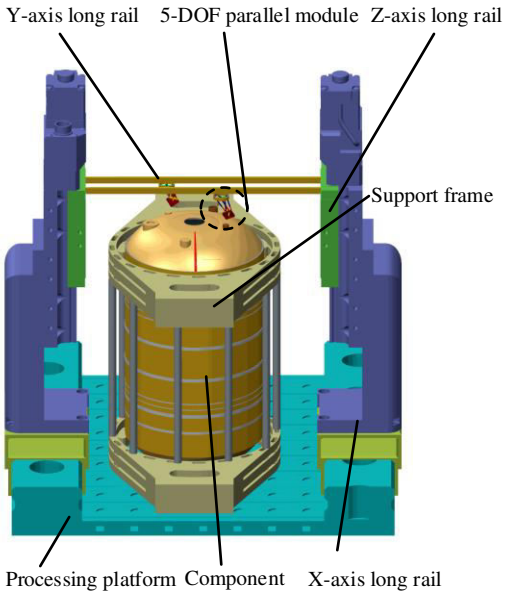

Figure 1 Hybrid removable robot and circumstance of super-large component

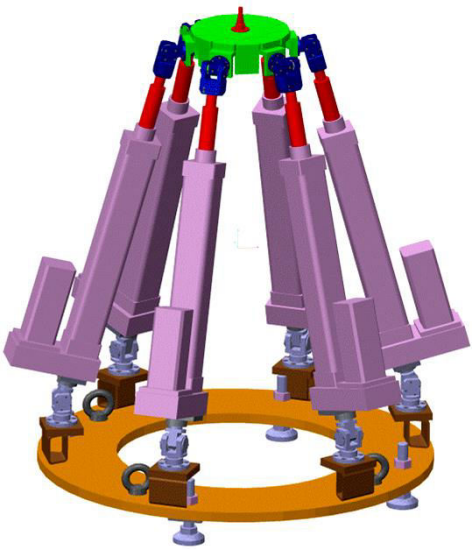

Figure 2 5-DOF parallel module

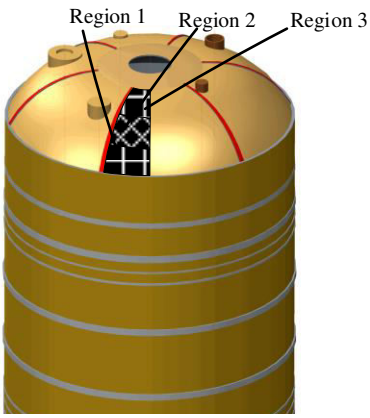

Figure 3 Shapes of segmented region

Nowadays, some scholars research some 5-DOF RAPMs. The redundantly actuated parallel mechanisms have fewer singularities, high fault tolerance, high stiffness than the traditional mechanisms. Such as, Yao et al. [10] analyzed dynamic and driving force optimization of the 5UPS-PRPU parallel mechanism, which is the redundantly actuated parallel mechanism and possesses high stiffness. UPS (S represents spherical joint, P represents prismatic joint and U represents universal joint) is an unconstrained limb. PRPU(R represents rotational joint) decides degrees of freedom of the parallel mechanism. Liu et al. [11] designed a 5-DOF parallel mechanism and analyzed dynamics with deformation compatibility of parallel mechanism, which is a 6PUS-UPU over-constrained parallel mechanism with high stiffness. The UPU limb decides degrees of freedom of the 6PUS-UPU RAPM, which have fewer singularities. Kang et al. [12] incorporated actuation redundancy into 5-DOF parallel mechanism, increased the load-carrying capacity of 5-DOF parallel mechanism, and avoided parallel singularities. Krut et al. [13] adopted rack-and-pinion systems as the moving platform and put forward Eureka RAPM. The parallel mechanism have high fault tolerance, and output angle of the moving platform can achieve $\pm 90^{o}$.

Some experts directly design the parallel mechanisms by arranging axis of the moving platform and achieve large output rotational angles of parallel mechanisms. Lian et al. [14] analyzed parameter sensitivity of the T5 parallel mechanism, which contains five UPS limbs and PaRot. Four symmetrical UPS limbs control the rotational angle of the parallel mechanism by means of the PaRot. O. Piccin et al. [15] proposed the architecture synthesis and designed a 5-DOF parallel mechanism by analyzing the kinematic decomposition of the task. Masouleh et al. [16] designed 5-RPRRR parallel mechanisms, which has larger output rotational angles by adopting R joint. Masouleh et al. [17–18] arranged axis of moving platform, analyzed the kinematics of the 5-RPUR parallel mechanisms and got the parallel mechanism with larger output rotational angle. Saadatzi et al. [19] used a geometric interpretation of the so-called vertex space and analyzed the workspace of the 5-PRUR parallel mechanisms, which possesses a large orientation workspace. Xie et al. [20] adopted the structure of icosahedrons and designed a 5-DOF parallel mechanism, which has large output rotational angles and is suitable for components with complicated surfaces. Viboon et al. [21] designed a 4-DOF parallel mechanism, which contains two kinematics limbs, and the axis of the rotational joint is non-collinear.

Some researchers proposed 5-DOF parallel mechanisms based on Lie group theory and computer-assisted. Ding et al. [22] established structure databases in computer and synthesized the 5-DOF parallel mechanisms, this computer-assisted method can design the symmetrical and asymmetrical parallel mechanisms, but it doesn't consider rotational angles of the parallel mechanisms. Wang et al. [23] proposed a class of 5-DOF parallel mechanisms (PMs) with properly constrained limb by topology design and analyzed the workspace of the properly constrained limb. The PMs have no singular position. Li et al. [24] synthesized 3R2T(T represents translation) parallel mechanisms by using the Lie group theory and proposed a general approach to design 5-DOF PMs, which is the symmetrical parallel mechanisms. Jin et al. [25] designed the articulated moving platform and synthesized 5-DOF parallel mechanisms by generalizing parallel mechanisms, which reach ±180°. But he did not consider the restriction of joint. Wang et al. [26] designed two moving platforms and synthesized a class of novel 2R3T and 2R2T parallel mechanisms with high rotational capability based on Lie group theory. The mechanism can realize large output rotational angles and be used in multi-axis 3D printing. Jin et al. [27] proposed two articulated moving platforms and synthesized a class of 4-DOF and 5-DOF parallel mechanisms, but all parallel mechanisms aren't suitable for processing super-large components with complicated surfaces.

One conclusion can be summarized based on the researches above that the RAPMs have fewer singularities, high fault tolerance than the traditional parallel mechanism. Most researchers directly designed exactly actuated parallel mechanisms or synthesized exactly actuated parallel mechanisms. But few scholars research 5-DOF redundantly actuated parallel mechanisms(RAPMs) with large output rotational angles Therefore, this paper will discuss 5-DoF synthesized RAPMs with large output rotational angles, and the parallel mechanism can be used in 5-DOF parallel module of 8-axis five linkage hybrid removable robot.

This paper focuses on type synthesis of the 5-DOF redundantly actuated parallel mechanisms for super-large components. First, a new machining scheme of 8-axis and 5-bar hybrid mobile robot with 5-DOF parallel module and 3 orthogonal long guide rails is proposed to solve the machining problem of super-large components with complex surfaces. Then, four kinds of RAMPs are presented by designing two articulated moving platforms and four kinds of limbs. The example RAPM is analyzed by closed-vector-circle method to solve the forward and inverse kinematic solution of the mechanism. Finally, a new trajectory planning method combining quadratic function with cosine is proposed and applied to restrain vibration impact of the RAPMs in movement. The results show the RAPM possesses large output rotational angles and verifies the efficiency of the trajectory planning method in movement.

The structure of this paper is as follows: Section 1 introduces a processing scheme of super-large components with complicated surfaces and research status. Four kinds of 5-DOF RAPMs are synthesized by designing two articulated moving platforms and four kinds of 5-DOF limbs in section 2. The example RAPM possesses larger output rotational angles, which is proved by analyzing the forward and inverse kinematic in section 3. A new trajectory planning method is proposed and applied to trajectory planning of the RAPM in industrial processes, the proposed method can make the RAPM in a steady-state in section 4. The conclusion is presented in section 5.

2 Design of RAPMs

Generally, The 5-DOF parallel mechanism should have five limbs, a moving platform, a fixed platform, and each limb has only one actuated joint. This paper presents the 5-DOF RAPM, which has six limbs, a moving platform, a fixed platform, and each limb has only one actuated joint, as shown in Figure 4. The moving platform should realize 5-DOF, namely 3T2R or 3R2T. The fixed platform includes 6 connection points.

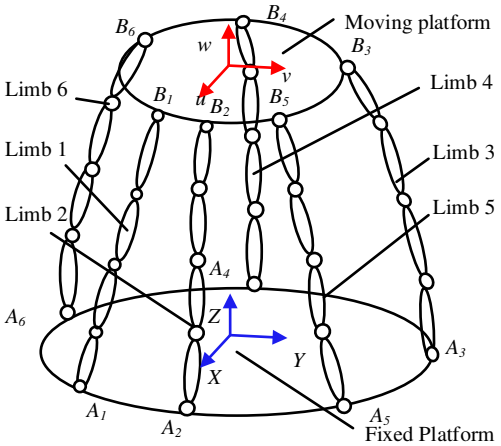

Figure 4 The 5-DOF redundantly actuated parallel mechanism

2.1 The moving platform

To realize the moving platform with large output rotational angles, the moving platform has four connection points, and four connection points combining the moving platform with six limbs shall be arranged symmetrically. The moving platform is simplified to a rectangle. The *o-uvw* is established at the center of the rectangle. *E*, *F*, *L*, and *M* are midpoints of edges of the rectangle, respectively. *GL*

and *QF* are vector that go straight down. *EJ* and *MH* are vector that go straight up, as shown in Figure 5, The rectangle rotates the *u*-axis along the arrow direction of *LG* and *EJ*, the rectangle rotates the *v*-axis along the arrow direction of *MH* and *FQ*.

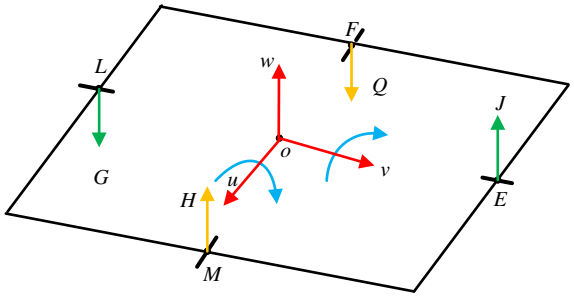

Figure 5 The moving platform

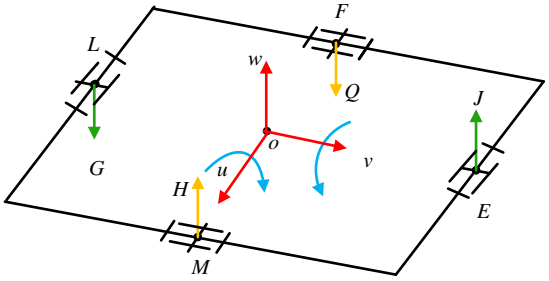

Figure 6(a) The articulated moving platform 1

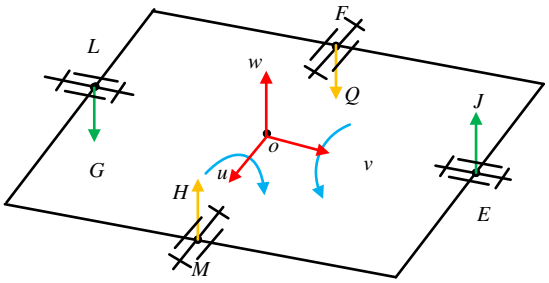

Figure 6(b) The articulated moving platform 2

Because of higher joints with small output rotational angles, such as universal joint, spherical joint, four revolute joints are installed at points *L*, *M*, *E*, and *F*. The rectangle is transformed into two rectangles, and the moving platform is transformed into two articulated moving platforms, as shown in Figure 6. The axis of the symmetric joints of the articulated moving platform 1 are parallel, and the axis of the symmetric joints of the articulated moving platform 2 is collinear.

2.2 The fixed platform

To realize the moving platform with large output rotational angles and force balance of parallel mechanism, the fixed platform has six connection points. The six connection points combining the fixed platform with six limbs shall be arranged symmetrically as shown in Figure 4.

2.3 The limb

2.3.1 Lie group theory

Lie group theory is one of type synthesis methods of parallel mechanism. Hervé [18] gives twelve classes of displacement subgroups, G(*u*) is one of twelve classes of displacement subgroups. G(*u*) represents that two-dimensional motion is perpendicular to the *u*-axis and one-dimensional rotation is rotated to the *u*-axis. G(*u*) is based on the characteristics of Li group theory and is shown in Table 1. G(*u*) is defined as an indivisible group, 5-DOF equivalent limbs are obtained by adding P joint or R joint to G(*u*), as shown in Table 2. {T(*u*)} (T represents translation), G(*u*), and {R(N_1,*v*)} (R represents rotation) can be swapped. The *u*, *v*, and *w* are the axis directions of the joints, and N_1, N_2, and N_3 are the positions of the joints.

2.3.2 Configuration evolution

Configuration evolution is a visible method to get new parallel mechanisms and depends on the existing parallel mechanisms. Fan [28] developed a planar 6R mechanism into some 4-DOF parallel mechanisms. Table 2 can be shown in Figure 7, and G(u) is added to 5-DOF equivalent limbs without changing five degrees of freedom, as shown in Figure 8.

Combined four evolution limbs with two articulated moving platforms, four evolution limbs can be evolved into 5-DOF equivalent evolution limbs without changing five degrees of freedom, so one limb is evolved into two limbs, as shown in Table 3.

Table 1 Kinematic limb of G(*u*)

Displacement subgroups	Kinematic limbs
R(N_1,*u*)R(N_2,u)R(N_3,u)	${}^{u}\mathrm{R}{}^{u}\mathrm{R}{}^{u}\mathrm{R}$
T(*v*)R(N_1,*u*)R(N_2,*u*)	${}^{v}\mathrm{P}{}^{u}\mathrm{R}{}^{u}\mathrm{R}$
R(N_1,*u*)T(*v*)R(N_2,u)	${}^{u}\mathrm{R}{}^{v}\mathrm{P}{}^{u}\mathrm{R}$
R(N_1,*u*)R(N_2,*u*)T(*v*)	${}^{u}\mathrm{R}{}^{u}\mathrm{R}{}^{v}\mathrm{P}$
R(N_1,*u*)T(*w*)T(*v*)	${}^{u}\mathrm{R}{}^{w}\mathrm{P}{}^{v}\mathrm{P}$
T(*w*)R(N_1,*u*)T(*v*)	${}^{w}\mathrm{P}{}^{u}\mathrm{R}{}^{v}\mathrm{P}$
T(*w*)T(*v*)R(N$_1$,*u*)	${}^{w}\mathrm{P}{}^{v}\mathrm{P}{}^{u}\mathrm{R}$

Table 2 5-DOF equivalent limbs

The 5-DOF limbs	Kinematic limbs
{T(*u*)}G(*u*){R(N_1,*v*)}	${}^{u}\mathrm{P}[{}^{v}\mathrm{P}{}^{w}\mathrm{P}{}^{u}\mathrm{R}]{}^{v}\mathrm{R}$
	${}^{u}\mathrm{P}[{}^{v}\mathrm{P}{}^{u}\mathrm{R}{}^{u}\mathrm{R}]{}^{v}\mathrm{R}$
	${}^{u}\mathrm{P}[{}^{u}\mathrm{R}{}^{u}\mathrm{R}{}^{u}\mathrm{R}]{}^{v}\mathrm{R}$
G(*u*){T(*u*)}{R(N_1,*v*)}	$[{}^{u}\mathrm{R}{}^{u}\mathrm{R}{}^{u}\mathrm{R}]{}^{u}\mathrm{P}{}^{v}\mathrm{R}$
	$[{}^{v}\mathrm{P}{}^{u}\mathrm{R}{}^{u}\mathrm{R}]{}^{u}\mathrm{P}{}^{v}\mathrm{R}$
	$[{}^{v}\mathrm{P}{}^{w}\mathrm{P}{}^{u}\mathrm{R}]{}^{u}\mathrm{P}{}^{v}\mathrm{R}$
{R(N_1,*v*)}{R(N_2,*v*)}G(*u*)	${}^{v}\mathrm{R}{}^{v}\mathrm{R}[{}^{u}\mathrm{R}{}^{u}\mathrm{R}{}^{u}\mathrm{R}]$
	${}^{v}\mathrm{R}{}^{v}\mathrm{R}[{}^{v}\mathrm{P}{}^{u}\mathrm{R}{}^{u}\mathrm{R}]$
	${}^{v}\mathrm{R}{}^{v}\mathrm{R}[{}^{v}\mathrm{P}{}^{w}\mathrm{P}{}^{u}\mathrm{R}]$
{R(N_1,*v*)}G(*u*){R(N_2,*v*)}	${}^{v}\mathrm{R}[{}^{u}\mathrm{R}{}^{u}\mathrm{R}{}^{u}\mathrm{R}]{}^{v}\mathrm{R}$

	^{v}R[^{v}P^{u}R^{u}R]^{v}R
	^{v}R[^{v}P^{w}P^{u}R]^{v}R

2.4 Type synthesis of RAPMs

To realize RAPMs with large output rotational angles, two identical limbs are positioned at *LG* and *EJ*, one same limb is positioned at *MH* and *FQ*, respectively, or one same limb is positioned at *LG* and *EJ*, two identical limbs are positioned at *MH* and *FQ*, respectively. The S joint can be shown as three orthogonal R joints. To get the large output rotational angle of the RAPM, the spherical joint is changed to a composite hinge, as shown in Figure 11.

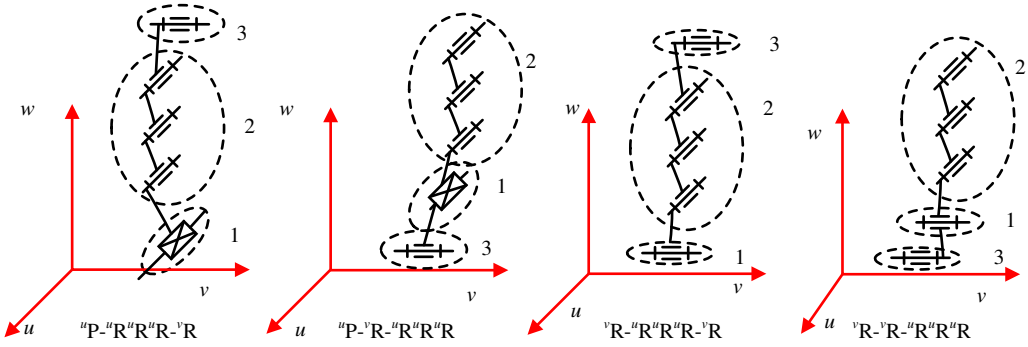

Figure 7 Four classes of 5-DOF equivalent limbs

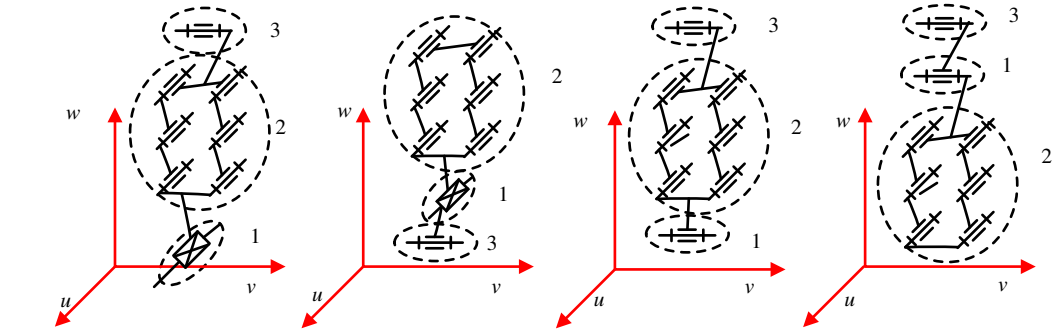

Figure 8 Four evolution limbs

Table 3 5-DOF equivalent evolution limbs

Limbs	Evolution limbs	Limbs	Evolution limbs
(a) ^{u}P-{^{u}R^{u}R^{u}R/^{u}R^{u}R^{u}R}-^{v}R	{^{u}P^{u}R^{u}R^{u}R/^{u}P^{u}R^{u}R^{u}R}-^{v}R	(c) ^{v}R-{^{u}R^{u}R^{u}R/^{u}R^{u}R^{u}R}-^{v}R	{^{v}U^{uu}R^{u}R/ ^{v}U^{uu}R^{u}R}-^{v}R
	{^{u}P^{w}P^{u}R^{u}R/^{u}P^{w}P^{u}R^{u}R}-^{v}R		{^{v}U^{uw}P^{u}R/ ^{v}U^{uw}P^{u}R}-^{v}R
	{^{u}P^{v}P^{w}P^{u}R/^{u}P^{v}P^{w}P^{u}R}-^{v}R		{^{v}U^{uv}P^{u}R/ ^{v}U^{uv}P^{u}R}-^{v}R
	{^{u}C^{u}R^{u}R/^{u}C^{u}R^{u}R}-^{v}R		{^{v}U^{uw}P^{v}P/ ^{v}U^{uw}P^{v}P}-^{v}R
	{^{u}C^{v}P^{u}R/^{u}C^{v}P^{u}R}-^{v}R		{^{v}U^{uv}P^{u}R/ ^{v}U^{uv}P^{u}R}-^{v}R
	{^{u}C^{w}P^{u}R/^{u}C^{w}P^{u}R}-^{v}R		{^{v}C^{uu}R^{u}R/ ^{v}C^{uu}R^{u}R}-^{v}R
	{^{u}C^{w}P^{v}P/^{u}C^{w}P^{v}P}-^{v}R		{^{v}C^{uw}P^{u}R/ ^{v}C^{uw}P^{u}R}-^{v}R
(b) {^{u}R^{u}R^{u}R/^{u}R^{u}R^{u}R}-^{u}P-^{v}R	{^{v}P^{w}P^{u}C/^{u}R^{w}P^{u}C}-^{v}R	(d){^{u}R^{u}R^{u}R/^{u}R^{u}R^{u}R}-^{v}R-^{v}R	{^{v}P^{u}R^{u}R^{v}R/^{v}P^{u}R^{u}R^{v}R}-^{v}R
	{^{u}R^{u}R^{u}C/^{u}R^{u}R^{u}C}-^{v}R		{^{w}P^{u}R^{u}R^{v}R/^{w}P^{u}R^{u}R^{v}R}-^{v}R
	{^{u}R^{v}P^{u}C/^{u}R^{v}P^{u}C}-^{v}R		{^{v}P^{w}P^{u}R^{v}R/^{v}P^{w}P^{u}R^{v}R}-^{v}R
	{^{v}P^{w}P^{u}C/^{v}P^{w}P^{u}C}-^{v}R		{^{u}R^{u}R^{u}U^{v}/^{u}R^{u}R^{u}U^{v}}-^{v}R
	{^{u}R^{v}P^{u}R^{u}P/^{u}R^{v}P^{u}R^{u}P}-^{v}R		{^{v}P^{u}R^{u}U^{v}/^{v}P^{u}R^{u}U^{v}}-^{v}R
	{^{u}R^{w}P^{u}R^{u}P/^{u}R^{w}P^{u}R^{u}P}-^{v}R		{^{w}P^{u}R^{u}U^{v}/^{w}P^{u}R^{u}U^{v}}-^{v}R
	{^{u}R^{v}P^{w}P^{u}P/^{u}R^{v}P^{w}P ^{u}P}-^{v}R		{^{w}P^{v}P^{u}U^{v}/^{w}P^{v}P^{u}U^{v}}-^{v}R

Methods 1. There are a constraint couple at the (a), (b), and (d) limbs, all constraint couples are parallel, but (c) limbs aren't parallel. Anyone of (a), (b), and (d) limbs is selected, and ^{v}R joint is connected to *LG* and *EJ*. Two UPS limbs are connected to *MH* and *FQ*, or anyone of (a), (b), and (d) limbs is selected, and ^{v}R joint is connected to *LG* and *EJ*. Two UPS limbs are connected to *MH* and *FQ*. All RAPMs combining the fixed platform with two articulated

moving platforms are shown in Table 4. Table 4 can be illustrated in Figure 10.

Methods 2. The RAPM is only based on the articulated platform 2. The articulated moving platform 2 is evolved into the new articulated moving platform, as shown in Figure 9. B_1, B_2, B_3, and B_4 are spherical joints. M and F position revolute joints, the axis of the revolute joints is collinear, L and E are revolute joints, the axis of the revolute joints is collinear, ^{v}R of each limb in Table 3 is connected to M and F. B_1, B_2, B_3, and B_4 connect to a spherical joint of UPS. All RAPMs combining the fixed platform with the articulated moving platforms 2 are shown in Table 5. Table 5 can be illustrated in Figure 11.

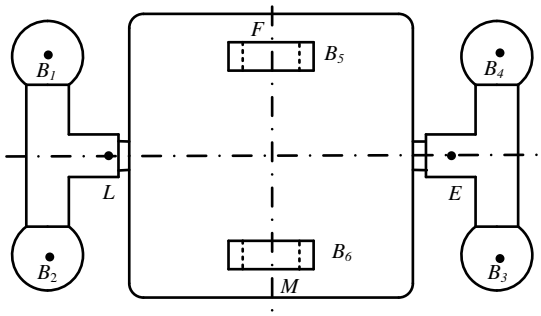

Figure 9 The new articulated moving platform

Table 4 Feasible limbs and the 5-DOF RAPMs

PM type	The limb *LG* and *EJ*	The limb *MH* and *FQ*	RAPMs
a	{^{u}P^{v}P^{u}R/^{u}P^{v}P^{u}R^{u}R}-^{v}R	UPS	2UPS+2{^{u}P^{v}P^{u}R^{u}R/^{u}P^{v}P^{u}R^{u}R}-^{v}R
	{^{u}P^{w}P^{u}R^{u}R/^{u}P^{w}P^{u}R^{u}R}-^{v}R		2UPS+2{^{u}P^{w}P^{u}R^{u}R/^{u}P^{w}P^{u}R^{u}R}-^{v}R
	{^{u}P^{v}P^{w}P^{u}R/^{u}P^{v}P^{w}P^{u}R}-^{v}R		2UPS+2{^{u}P^{v}P^{w}P^{u}R/^{u}P^{v}P^{w}P^{u}R}-^{v}R
	{^{u}C^{u}R^{u}R/^{u}C^{u}R^{u}R}-^{v}R		2UPS+2{^{u}C^{u}R^{u}R/^{u}C^{u}R^{u}R}-^{v}R
	{^{u}C^{v}P^{u}R/^{u}C^{v}P^{u}R}-^{v}R		2UPS+2{^{u}C^{v}P^{u}R/^{u}C^{v}P^{u}R}-^{v}R
	{^{u}C^{w}P^{u}R/^{u}C^{w}P^{u}R}-^{v}R		2UPS+2{^{u}C^{w}P^{u}R/^{u}C^{w}P^{u}R}-^{v}R
	{^{u}C^{w}P^{v}P/^{u}C^{w}P^{v}P}-^{v}R		2UPS+2{^{u}C^{w}P^{v}P/^{u}C^{w}P^{v}P}-^{v}R
b	{^{v}P^{w}P^{u}C/^{u}R^{w}P^{u}C}-^{v}R	UPS	2UPS+{^{v}P^{w}P^{u}C/^{u}R^{w}P^{u}C}-^{v}R
	{^{u}R^{u}R^{u}C/^{u}R^{u}R^{u}C}-^{v}R		2UPS+2{^{u}R^{u}R^{u}C/^{u}R^{u}R^{u}C}-^{v}R
	{^{u}R^{v}P^{u}C/^{u}R^{v}P^{u}C}-^{v}R		2UPS+2{^{u}R^{v}P^{u}C/^{u}R^{v}P^{u}C}-^{v}R
	{^{v}P^{w}P^{u}C/^{v}P^{w}P^{u}C}-^{v}R		2UPS+{^{v}P^{w}P^{u}C/^{v}P^{w}P^{u}C}-^{v}R
	{^{u}R^{v}P^{u}R^{u}P/^{u}R^{v}P^{u}R^{u}P}-^{v}R		2UPS+2{^{u}R^{v}P^{u}R^{u}P/^{u}R^{v}P^{u}R^{u}P}-^{v}R
	{^{u}R^{w}P^{u}R^{u}P/^{u}R^{w}P^{u}R^{u}P}-^{v}R		2UPS+2{^{u}R^{w}P^{u}R^{u}P/^{u}R^{w}P^{u}R^{u}P}-^{v}R
	{^{u}R^{v}P^{w}P^{u}P/^{u}R^{v}P^{w}P^{u}P}-^{v}R		2UPS+2{^{u}R^{v}P^{w}P^{u}P/^{u}R^{v}P^{w}P^{u}P}-^{v}R
d	{^{v}P^{u}R^{v}R/^{v}P^{u}R^{v}R}-^{v}R	UPS	2UPS+2{^{v}P^{u}R^{v}R/^{v}P^{u}R^{v}R}-^{v}R
	{^{w}P^{u}R^{v}R/^{w}P^{u}R^{v}R}-^{v}R		2UPS+2{^{w}P^{u}R^{v}R/^{w}P^{u}R^{v}R}-^{v}R
	{^{v}P^{w}P^{u}R^{v}R/^{v}P^{w}P^{u}R^{v}R}-^{v}R		2UPS+2{^{v}P^{w}P^{u}R^{v}R/^{v}P^{w}P^{u}R^{v}R}-^{v}R
	{^{u}R^{u}R^{u}U^{v}/^{u}R^{u}R^{u}U^{v}}-^{v}R		2UPS+2{^{u}R^{u}R^{u}U^{v}/^{u}R^{u}R^{u}U^{v}}-^{v}R
	{^{v}P^{u}R^{u}U^{v}/^{v}P^{u}R^{u}U^{v}}-^{v}R		2UPS+2{^{v}P^{u}R^{u}U^{v}/^{v}P^{u}R^{u}U^{v}}-^{v}R
	{^{w}P^{u}R^{u}U^{v}/^{w}P^{u}R^{u}U^{v}}-^{v}R		2UPS+2{^{w}P^{u}R^{u}U^{v}/^{w}P^{u}R^{u}U^{v}}-^{v}R
	{^{w}P^{v}P^{u}U^{v}/^{w}P^{v}P^{u}U^{v}}-^{v}R		2UPS+2{^{w}P^{v}P^{u}U^{v}/^{w}P^{v}P^{u}U^{v}}-^{v}R
	{^{v}P^{u}R^{v}R/^{v}P^{u}R^{v}R}-^{v}R		2UPS+2{^{v}P^{u}R^{v}R/^{v}P^{u}R^{v}R}-^{v}R
	{^{w}P^{u}R^{v}R/^{w}P^{u}R^{v}R}-^{v}R		2UPS+2{^{w}P^{u}R^{v}R/^{w}P^{u}R^{v}R}-^{v}R
	{^{v}P^{w}P^{u}R^{v}R/^{v}P^{w}P^{u}R^{v}R}-^{v}R		2UPS+2{^{v}P^{w}P^{u}R^{v}R/^{v}P^{w}P^{u}R^{v}R}-^{v}R

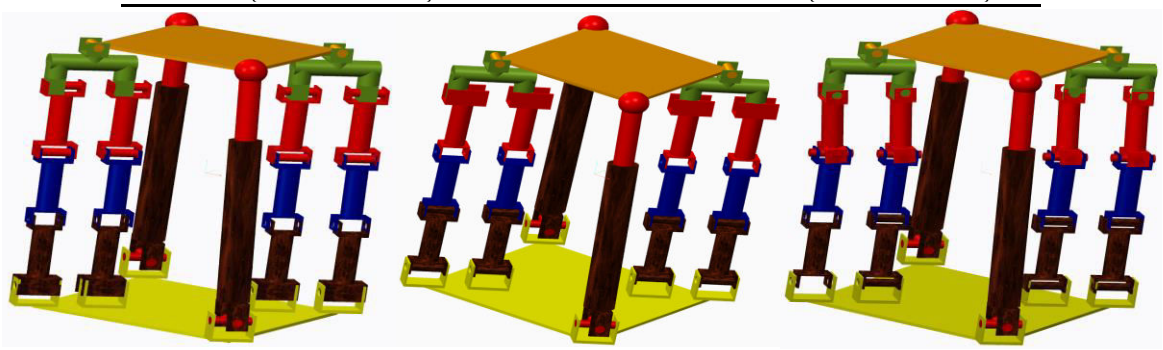

a b d

Figure 10 Three kinds of the 5-DOF RAPMs

Table 5 Feasible limbs and the 5-DOF RAPMs

PM type	The limb B_5 and B_6	The limb B_1, B_2, B_3 and B_4	RAPMs
a	{“P^{v}P“R“R/“P^{v}P“R“R}-^{v}R	UPS	4UPS+{“P^{v}P“R“R/“P^{v}P“R“R}-^{v}R
	{“P^{w}P“R“R/“P^{w}P“R“R}-^{v}R		4UPS+{“P^{w}P“R“R/“P^{w}P“R“R}-^{v}R
	{“P^{v}P^{w}P“R/“P^{v}P^{w}P“R}-^{v}R		4UPS+{“P^{v}P^{w}P“R/“P^{v}P^{w}P“R}-^{v}R
	{“C“R“R/“C“R“R}-^{v}R		4UPS+{“C“R“R/“C“R“R}-^{v}R
	{“C^{v}P“R/“C^{v}P“R}-^{v}R		4UPS+{“C^{v}P“R/“C^{v}P“R}-^{v}R
	{“C^{w}P“R/“C^{w}P“R}-^{v}R		4UPS+{“C^{w}P“R/“C^{w}P“R}-^{v}R
	{“C^{w}P^{v}P/“C^{w}P^{v}P}-^{v}R		4UPS+{“C^{w}P^{v}P/“C^{w}P^{v}P}-^{v}R
	{^{v}P^{w}P“C/“R^{w}P“C}-^{v}R	UPS	4UPS+{^{v}P^{w}P“C/“R^{w}P“C}-^{v}R
b	{“R“R“C/“R“R“C}-^{v}R		4UPS+{“R“R“C/“R“R“C}-^{v}R
	{“R^{v}P“C/“R^{v}P“C}-^{v}R		4UPS+{“R^{v}P“C/“R^{v}P“C}-^{v}R
	{^{v}P^{w}P“C/^{v}P^{w}P“C}-^{v}R		4UPS+{^{v}P^{w}P“C/^{v}P^{w}P“C}-^{v}R
	{“R^{v}P“R“P/“R^{v}P“R“P}-^{v}R		4UPS+{“R^{v}P“R“P/“R^{v}P“R“P}-^{v}R
	{“R^{w}P“R“P/“R^{w}P“R“P}-^{v}R		4UPS+{“R^{w}P“R“P/“R^{w}P“R“P}-^{v}R
	{“R^{v}P^{w}P“P/“R^{v}P^{w}P “P}-^{v}R		4UPS+{“R^{v}P^{w}P“P/“R^{v}P^{w}P “P}-^{v}R
c	{^{v}U^{uu}R“R/ ^{v}U^{uu}R“R}-^{v}R	UPS	4UPS+{^{v}U^{uu}R“R/ ^{v}U^{uu}R“R}-^{v}R
	{^{v}U^{uw}P“R/ ^{v}U^{uw}P“R}-^{v}R		4UPS+{^{v}U^{uw}P“R/ ^{v}U^{uw}P“R}-^{v}R
	{^{v}U^{uv}P“R/ ^{v}U^{uv}P“R}-^{v}R		4UPS+{^{v}U^{uv}P“R/ ^{v}U^{uv}P“R}-^{v}R
	{^{v}U^{uw}P^{v}P/ ^{v}U^{uw}P^{v}P}-^{v}R		4UPS+{^{v}U^{uw}P^{v}P/ ^{v}U^{uw}P^{v}P}-^{v}R
	{^{v}U^{uv}P“R/ ^{v}U^{uv}P“R}-^{v}R		4UPS+{^{v}U^{uv}P“R/ ^{v}U^{uv}P“R}-^{v}R
	{^{v}C^{uu}R“R/ ^{v}C^{uu}R“R}-^{v}R		4UPS+{^{v}C^{uu}R“R/ ^{v}C^{uu}R“R}-^{v}R
	{^{v}C^{uw}P“R/ ^{v}C^{uw}P“R}-^{v}R		4UPS+{^{v}C^{uw}P“R/ ^{v}C^{uw}P“R}-^{v}R
d	{^{v}P“R“R^{v}R/^{v}P“R“R^{v}R}-^{v}R	UPS	4UPS+{^{v}P“R“R^{v}R/^{v}P“R“R^{v}R}-^{v}R
	{^{w}P“R“R^{v}R/^{w}P“R“R^{v}R}-^{v}R		4UPS+{^{w}P“R“R^{v}R/^{w}P“R“R^{v}R}-^{v}R
	{^{v}P^{w}P“R^{v}R/^{v}P^{w}P“R^{v}R}-^{v}R		4UPS+{^{v}P^{w}P“R^{v}R/^{v}P^{w}P“R^{v}R}-^{v}R
	{“R“R“U^{v}/“R“R“U^{v}}-^{v}R		4UPS+{“R“R“U^{v}/“R“R“U^{v}}-^{v}R
	{^{v}P“R“U^{v}/^{v}P“R“U^{v}}-^{v}R		4UPS+{^{v}P“R“U^{v}/^{v}P“R“U^{v}}-^{v}R
	{^{w}P“R“U^{v}/^{w}P“R“U^{v}}-^{v}R		4UPS+{^{w}P“R“U^{v}/^{w}P“R“U^{v}}-^{v}R
	{^{w}P^{v}P“U^{v}/^{w}P^{v}P“U^{v}}-^{v}R		4UPS+{^{w}P^{v}P“U^{v}/^{w}P^{v}P“U^{v}}-^{v}R
	{^{v}P“R“R^{v}R/^{v}P“R“R^{v}R}-^{v}R		4UPS+{^{v}P“R“R^{v}R/^{v}P“R“R^{v}R}-^{v}R
	{^{w}P“R“R^{v}R/^{w}P“R“R^{v}R}-^{v}R		4UPS+{^{w}P“R“R^{v}R/^{w}P“R“R^{v}R}-^{v}R
	{^{v}P^{w}P“R^{v}R/^{v}P^{w}P“R^{v}R}-^{v}R		4UPS+{^{v}P^{w}P“R^{v}R/^{v}P^{w}P“R^{v}R}-^{v}R

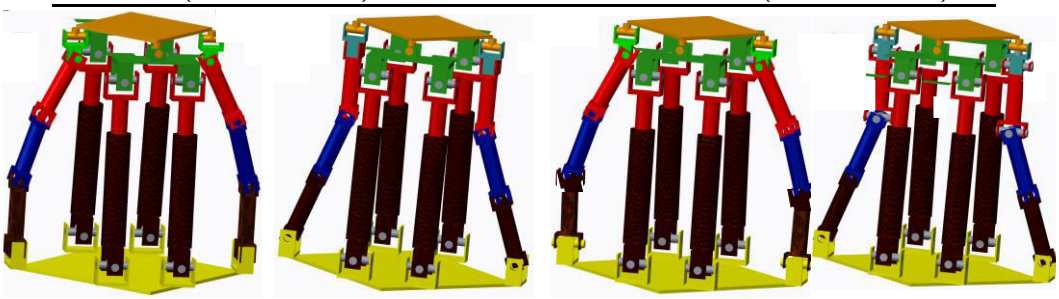

a b c d

Figure 11 Four kinds of the 5-DOF RAPMs

3 Kinematics analysis

3.1 Structure description

The RAPM is selected as the parallel module of the hybrid removable robot according to the following criteria: 1, the actuated joint should be attached to the fixed platform or nearby the fixed platform as far as possible. 2, the prismatic joint is selected as the actuated joint. 3, the direction of the actuated joint should be close as possible

to the vertical direction of the fixed platform. So the example 4UPS+{^{v}U^{uw}P^{u}R/^{v}U^{uw}P^{u}R}-^{v}R is more suitable for the parallel module, as shown in Figure 12. 4UPS+{^{v}U^{uw}P^{u}R/^{v}U^{uw}P^{u}R}-^{v}R contains six limbs, the articulated moving platform, the fixed platform. The {^{v}U^{uw}P^{u}R/ ^{v}U^{uw}P^{u}R}-^{v}R contains two limbs. *M* and *F* share ^{v}R. 4UPS+{^{v}U^{uw}P^{u}R/^{v}U^{uw}P^{u}R}-^{v}R is a 5-DOF RAPM, and the 5-DOF RAPM can't rotate about the normal of the articulated platform.

The *O-XYZ* is established at the center of the fixed platform, the *o-uvw* is established at the center of the articulated moving platform. A_1, A_2, A_3, A_4, A_5, and A_6 are evenly distributed on the fixed platform. B_1, B_2, B_3, B_4, B_5, and B_6 are evenly distributed on the articulated moving platform. A_5 and A_6 are on the *OY*-axis, B_5 and B_6 are on the ov-axis. The distance between A_i(i=1~6) and *O* is R_1(R_1 represents radius). The distance between B_i and o is r_1(r_1 represents radius). The length of the limb is l_i. Prismatic joint of each limb is the actuated joint. All parameters is shown in Table 6.

3.2 Establishment of kinematic model

The 1, 2, 3, and 4 limbs have position function when the RAPM rotates along the ou-axis, and the 5 and 6 limbs control the rotation of the articulated moving platform along the *ou*-axis. The 5 and 6 limbs have position function when the RAPM rotates along the *ov*-axis, and the 1, 2, 3, and 4 limbs control the rotation of the articulated moving platform along the *ov*-axis.

The *O* point in coordinate system *O-XYZ* is $(0, 0, 0)^{T}$. The o point in coordinate system *O-XYZ* is $(x, y, z)^{T}$, and it is expressed as $^{O}\boldsymbol{o}=(x, y, z)^{T}$. α is alpha and represents the rotational angle about *X*-axis, β is beta and represents the rotational angle about *Y*-axis. The rotational matrix of the RAPM is expressed as

$$R=\begin{bmatrix}\cos\beta & \sin\alpha\sin\beta & \cos\alpha\sin\beta\\ 0 & \cos\alpha & -\sin\alpha\\ -\sin\beta & \sin\alpha\cos\beta & \cos\alpha\cos\beta\end{bmatrix} \tag{1}$$

A_i is expressed in *O-XYZ*, B_i is expressed in *o-uvw*, as shown in Table 6. The coordinates of B_i in *O-XYZ* are expressed as

$$^{O}\boldsymbol{B}_i=^{O}\boldsymbol{o}+R^{o}\boldsymbol{B}_i. \tag{2}$$

The length vector of the limbs in *O-XYZ* is expressed as

$$\boldsymbol{l}_i=^{O}\boldsymbol{A}_i-^{O}\boldsymbol{B}_i. \tag{3}$$

The A_iB_ioO closed-loop vector equation in *O-XYZ* is written as

$$\boldsymbol{Oo}+\boldsymbol{oB}_i=\boldsymbol{OA}_i+\boldsymbol{A}_i\boldsymbol{B}_i\ (i=1\sim6) \tag{4}$$

where $\boldsymbol{Oo}=^{O}\boldsymbol{o}$, $\boldsymbol{OA}_i=\|R_1\|$, $\boldsymbol{A}_i\boldsymbol{B}_i=q_iw_i=\boldsymbol{l}_i$, $\boldsymbol{B}_i\boldsymbol{o}=-R^{o}\boldsymbol{B}_i$. q_i is the length of the chain *i*, w_i is unit vector direction of the chain *i*.

Equation of each limb is written as

$$\begin{cases} q_i=\left|{}^{O}\boldsymbol{o}+\boldsymbol{oB}_i-\boldsymbol{OA}_i\right| \\ w_i=\dfrac{{}^{O}\boldsymbol{o}+\boldsymbol{oB}_i-\boldsymbol{OA}_i}{q_i} \end{cases} \quad i=1\sim6\,. \tag{5}$$

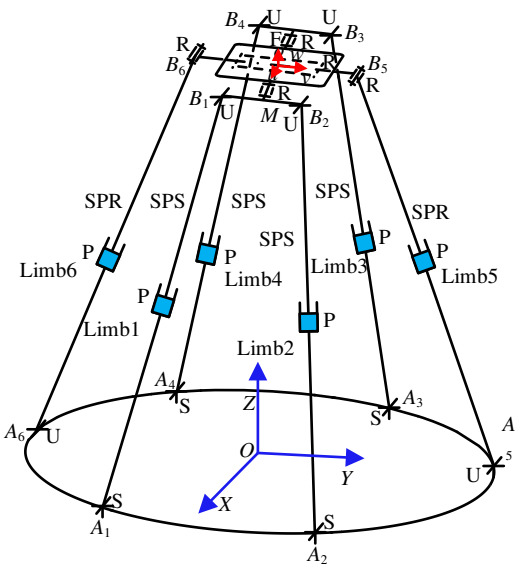

Figure 12 4UPS+{S^{w}P^{u}R/ S^{w}P^{u}R}-^{v}R RAPM

3.3 Velocity analysis

The velocity relationship between the P actuated joint and the center *o* is obtained by taking the derivative of equation (4).

$$v_{Bi}=v+\omega\times(R^{o}B_i)=\dot{q}_iw_i+q_i\omega_i\times w_i \tag{6}$$

where *v* is the linear velocity of *o*, ω is angular velocity of *o*, ω_i is angular velocity of the kinematic chain *i*, $\dot{q}_i$ is velocity of the P actuated joint.

$S(w_i)$ and $S(B_i)$ are anti-symmetric matrices and are written as

$$S(w_i)=\begin{bmatrix}0 & -w_{iz} & w_{iy}\\ w_{iz} & 0 & -w_{ix}\\ -w_{iy} & w_{ix} & 0\end{bmatrix}\ S(B_i)=\begin{bmatrix}0 & -B_{iz} & B_{iy}\\ B_{iz} & 0 & -B_{ix}\\ -B_{iy} & B_{ix} & 0\end{bmatrix}$$

Both sides of equation (6) crossing w_i, the angular velocity of the kinematic chain *i* is obtained.

$$\omega_i=\frac{w_i\times v_{Bi}}{q_i}=\frac{S(w_i)}{q_i}v_{Bi}=J_{wi}\begin{bmatrix}v\\ \omega\end{bmatrix} \tag{7}$$

where $J_{wi}=\dfrac{S(w_i)}{q_i}$.

Both sides of equation (6) multiplying w_i, the P actuated velocity is obtained

$$\dot{q}_i=\begin{bmatrix}w_i^{T} & ((R^{o}B_i)\times w_i)^{T}\end{bmatrix}\begin{bmatrix}v\\ \omega\end{bmatrix}=J_{qi}\begin{bmatrix}v\\ \omega\end{bmatrix}=J_{qi}v_s \tag{8}$$

where J_{qi} is the Jacobi matrix of the actuated joint of RAPMs.

The relationship between the rotational velocity in the Cartesian coordinates system and the rotational velocity in

the generalized coordinate system is represented as

$$\omega=\begin{bmatrix}1 & 0 & \sin\beta\\ 0 & \cos\alpha & -\sin\alpha\\ 0 & \sin\alpha & \cos\alpha\cos\beta\end{bmatrix}\begin{bmatrix}\dot{\alpha}\\ \dot{\beta}\\ \dot{\gamma}\end{bmatrix}=J_{\omega}v_s \tag{9}$$

The six-dimensional velocity of the moving platform is represented as

$$\begin{bmatrix}v\\ \omega\end{bmatrix}=\begin{bmatrix}J_v\\ J_{\omega}\end{bmatrix}v_s=J_0v_s \tag{10}$$

where $J_0=\begin{bmatrix}1&0&0&0&0&0\\0&1&0&0&0&0\\0&0&1&0&0&0\\0&0&0&1&0&\sin\beta\\0&0&0&0&\cos\alpha&-\sin\alpha\\0&0&0&0&\sin\alpha&\cos\alpha\cos\beta\end{bmatrix}$.

The Jacobi matrix between the velocity of the P actuated joint and output velocity of the mechanism in the generalized coordinate system is written as

$$J=J_{qi}J_0 \tag{11}$$

The velocity relationship between the P actuated joint and the center o in the generalized coordinate system is written as

$$\dot{q}_i=Jv_s \tag{12}$$

3.4 Acceleration analysis

The linear velocity of B_i is written as

$$v_{Bi}=v+\omega\times(R\cdot{}^oB_i)=\begin{bmatrix}I_{3*3} & -S(B_i)\end{bmatrix}\begin{bmatrix}v\\ \omega\end{bmatrix}=J_{ri}\begin{bmatrix}v\\ \omega\end{bmatrix} \tag{13}$$

where $J_{ri}=\begin{bmatrix}I_{3*3} & -S(B_i)\end{bmatrix}$.

The acceleration of B_i is obtained by taking derivative of equation (6).

$$\dot{v}_{Bi}=\dot{v}+\dot{\omega}\times(R\cdot{}^oB_i)+\omega\times(\omega\times(R\cdot{}^oB_i)) \tag{14}$$

$$\dot{v}_{Bi}=\ddot{q}_iw_i+2*\dot{q}_i\omega_i\times w_i+q_i\dot{\omega}_i\times w_i+q_i\omega_i\times(\omega_i\times w_i) \tag{15}$$

Both sides of equation (6) multiplying w_i, the P actuated velocity is obtained.

$$\dot{q}_i=w_i^T\cdot v_{Bi} \tag{16}$$

The linear acceleration of the P actuated joint is obtained by taking the derivative of equation (16).

$$\ddot{q}_i=w_i^T\dot{v}_{Bi}+v_{Bi}^T(\omega_i\times w_i)=J[a\quad \varepsilon]^T+K_{li}[v\quad \omega]^T \tag{17}$$

where a is the linear acceleration of o, ε is angular acceleration of o.

$K_{li}=w_i^T\cdot\dot{J}_{ri}-[J_{ri}[v\quad w]^T]^T\cdot S(w_i)\cdot J_{wi}$.

3.5 Kinematics Performance analysis

The output rotational angle is one of the important indexes to evaluate the performance of the RAPM, it is necessary to evaluate the RAPM with the output rotational angle. In practical application, the length of the limbs and the angle of the joints are somewhat limited. The S joint can be shown as three orthogonal R joint. To get the large output rotational angle of the RAPM, the spherical joint is changed to a composite hinge, as shown in Figure 13. The parameters of the RAPM in Figure 13 are shown in Table 6. The flow chart of the reachable workspace is shown in Figure 14. The reachable workspace of the RAPM can be gotten by border limiting method and based on the parameters of Table 6, as shown in Figure 15.

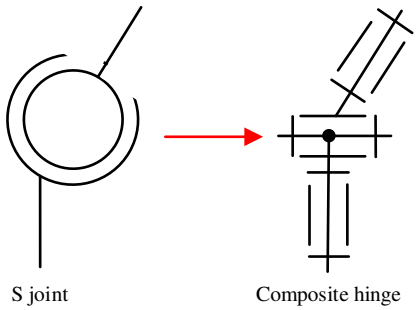

Figure 13 S joint and composite hinge

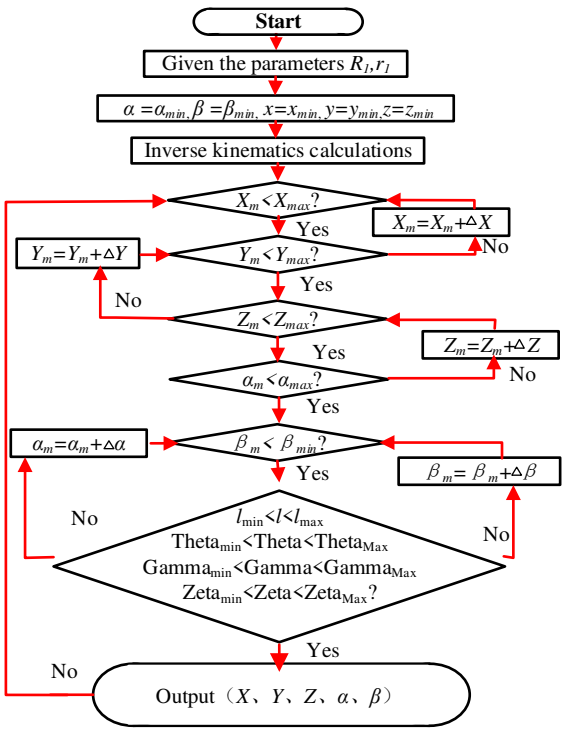

Figure 14 Flow chart for the reachable workspace

Table 6 Structural and physical parameters

Parameter	Description	Value	Unit
R_1	Radius of the fixed platform	600	mm
r_1	Radius of the moving platform	300	mm

A_1	A_1 in *O-XYZ*	($\sqrt{3}$ R_1/2, - R_1/2,0)	mm
A_2	A_2 in *O-XYZ*	($\sqrt{3}$ R_1/2, R_1/2,0)	mm
A_3	A_3 in *O-XYZ*	(-$\sqrt{3}$ R_1/2, R_1/2,0)	mm
A_4	A_4 in *O-XYZ*	(-$\sqrt{3}$ R_1/2, - R_1/2,0)	mm
A_5	A_5 in *O-XYZ*	(0, R_1,0)	mm
A_6	A_6 in *O-XYZ*	(0,- R_1,0)	mm
B_1	B_1 in *o-uvw*	($\sqrt{3}$ r_1/2, - r_1/2,0)	mm
B_2	B_2 in *o-uvw*	($\sqrt{3}$ r_1/2, r_1/2,0)	mm
B_3	B_3 in *o-uvw*	(-$\sqrt{3}$ r_1/2, r_1/2,0)	mm
B_4	B_4 in *o-uvw*	(-$\sqrt{3}$ r_1/2, - r_1/2,0)	mm
B_5	B_5 in *o-uvw*	(0, r_1,0)	mm
B_6	B_6 in *o-uvw*	(0, -r_1,0)	mm
l_{min}	The minimum length of limb	500	mm
l_{max}	The maximum length of limb	1000	mm
$Theta_{max}$	The maximum cosine of R joint (SPR) and R joint (H)	0.866	
$Theta_{min}$	The minimum cosine of R joint (SPR) and R joint(H)	-1	
$Zeta_{min}$	The minimum cosine of S joint (SPR) and fixed platform	0.866	
$Zeta_{max}$	The maximum cosine of S joint (SPR) and fixed platform	-0.866	
$Gamma_{min}$	The minimum cosine of S joint (SPS) and moving platform	-0.866	
$Gamma_{max}$	The maximum cosine of S joint (SPS) and moving platform	0.866	

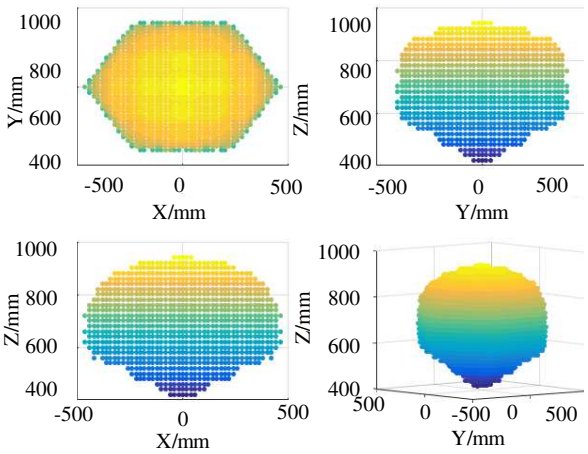

Figure 15 The workspace of the RAPM

As can be seen from Figure 15, X changes from -480mm to 480mm, Y changes from -400mm to 400mm, and Z changes from 420mm to 900mm. The workspace of the RAPM is symmetrical about *OXZ* and *OYZ*. The mechanism can reach the maximum movement in the *OXY* plane when Z is 620mm. At the same time, the Z-alpha-beta orientation workspace can be obtained and be shown in Figure 16, and the relationship between alpha and beta can be obtained and be shown in Figure 17 when Z is different values.

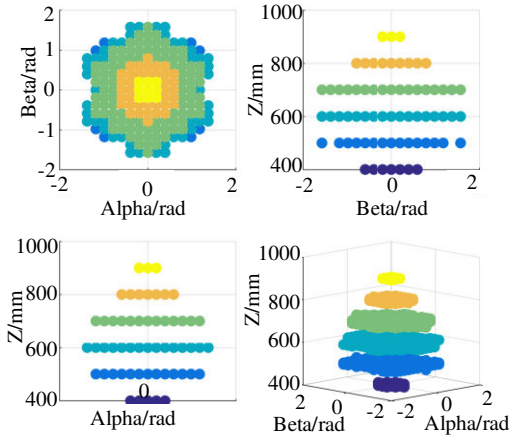

Figure 16 Z-alpha-beta orientation workspace

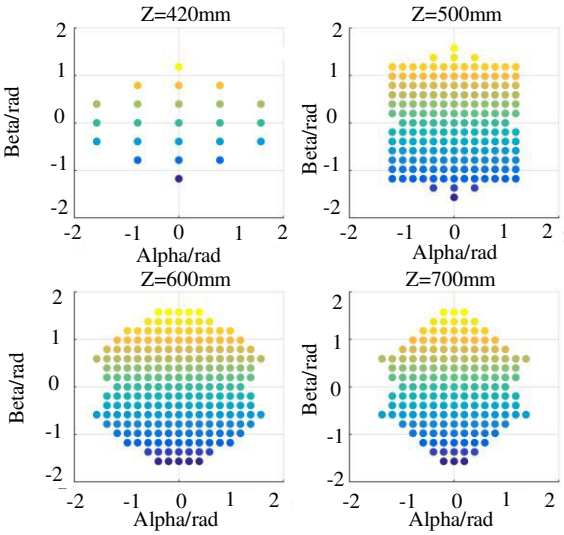

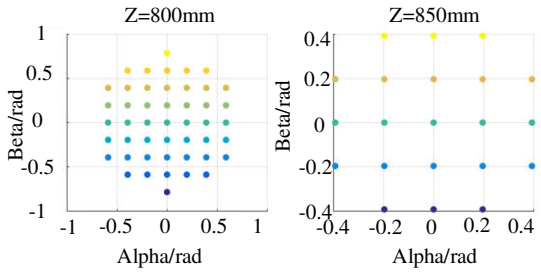

Figure 17 Alpha and beta at different Z values

According to Figure 16 and Figure 17, alpha and beta change from small to big, then from big to small when Z changes from small to big. The RAPM can reach 90° when Z is 620mm. the RAPMs with large output rotational angles can be obtained on the basis of configuration evolution and Li group theory.

4 Motion simulation

4.1 Trajectory planning of RAPMs

To ensure the machining accuracy of super-large components with complicated surfaces, the parallel mechanism should move smoothly and have no vibration impact. To verify the kinematic ability of the parallel mechanism and avoid vibration impact of the parallel mechanism in movement, many researchers proposed own trajectory planning methods [29–39]. The vibration impact of the mechanism is more likely to damage the parallel mechanism and can be represented by the continuity of acceleration. This paper represents own method to eliminate vibration impact of the parallel mechanism in movement, it is necessary to the trajectory planning of the parallel mechanism in the machining process. Based on the machining tasks, the continuous linear motion trajectory planning simulation of the mechanism is carried out. The goal of trajectory planning is that the RAPMs have no vibration impact in the minimum time. The dimension parameters of the super-large component is reduced, and the trajectory of the processing task is shown in Figure 16. P_1P_2 is a straight line. P_2P_3 is a circular arc line. P_3P_4 is a straight line. P_4P_5 is made up of many arcs line. Key points of machining trajectory should be considered as follows: 1, the RAPM should avoid the interference surface in the route; 2, the RAPM should have been in a steady-state and can't have mechanism impact. The parameters of P_i (i =1~5) are shown in Table 7.

Table 7 The parameters of P_i

Path point	Coordinate /mm	Description
P_1	(0,-650,400)	starting point
P_2	(0,-650,100)	key point
P_3	(0,-550,0)	key point
P_4	(0,-500,0)	reference point
P_5	(0, 0,300)	end point

The trajectories from P_1 to P_5 in Figure 18 is shown in Figure 19. P_1P_2 in Figure 18 represents P_1P_2 in Figure 19. P_2P_3 in Figure 18 represents P_2P_3 in Figure 19. P_3P_4 in Figure 18 represents P_3P_4 in Figure 19. P_4P_5 in Figure 18 represents P_2P_3 in Figure 19. If the RAMPs can realize the trajectory in Figure 18, the RAMPs can also complete the trajectory in Figure 19. The time from P_1 to P_2 is t_{11}, the time from P_2 to P_3 is t_{22}, the time from P_3 to P_4 is t_{33}, the time from P_1 to P_3 is t_{44}.

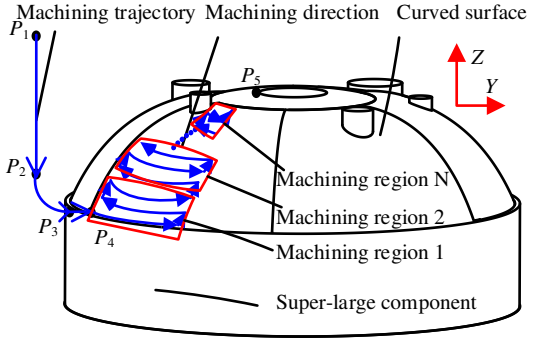

Figure 18 The machining trajectory and the super-large component.

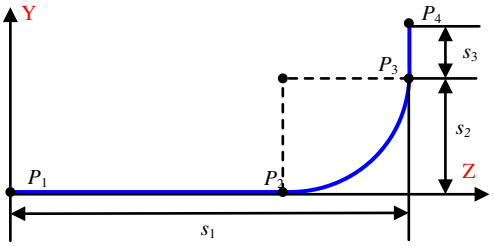

Figure 19 Simplified trajectories of the RAPMs

4.1.1 The proposed trajectory planning method for operating space

To make the RAPMs without mechanical vibration impact in the minimum time, a new method combining quadratic function with cosine is proposed and applied to acceleration of the RAPMs, as shown in Figure 20. The cosine function-constant planning method contains four phases, such as, the accelerated acceleration, steady acceleration, the reduced acceleration, constant velocity.

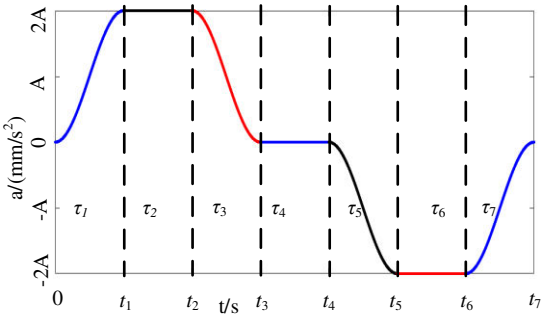

Figure 20 The cosine function-constant planning method

Kinematic velocity of the RAPMs should be zero at the

starting period and ending period. τ_k is k duration, τ_1 and τ_5 are accelerated acceleration period, τ_2 and τ_6 are steady acceleration period, τ_3 and τ_7 are reduced acceleration period, τ_4 is constant velocity period. The acceleration equations of the cosine function-constant planning method based on Figure 20 are expressed as

$$a=\begin{cases} A-A\cos(\omega_1 t) & 0<t<t_1 \\ 2A & t_1<t<t_2 \\ A+A\cos(\omega_2(t-t_2)) & t_2<t<t_3 \\ 0 & t_3<t<t_4 \\ -A+A\cos(\omega_3(t-t_4)) & t_4<t<t_5 \\ -2A & t_5<t<t_6 \\ -A-A\cos(\omega_4(t-t_6)) & t_6<t<t_7 \end{cases} \tag{16}$$

where ω_1, ω_2, ω_3 and ω_4 is coefficient; A is amplitude; t_1, t_2, t_3, t_4, t_5, t_6 and t_7 are time.

The velocity is obtained by integrating the acceleration, velocity equations (17) are expressed as

$$v=\begin{cases} At+C_1-A\sin(\omega_1 t)/\omega_1 & 0<t<t_1 \\ 2At+C_2 & t_1<t<t_2 \\ At+C_3+A\sin(\omega_2(t-t_2))/\omega_2 & t_2<t<t_3 \\ C_4 & t_3<t<t_4 \\ -At+C_5+A\sin(\omega_3(t-t_4))/\omega_3 & t_4<t<t_5 \\ -2At+C_6 & t_5<t<t_6 \\ -At+C_7-A\sin(\omega_4(t-t_6))/\omega_4 & t_6<t<t_7 \end{cases} \tag{17}$$

where C_1, C_2, C_3, C_4, C_5, C_6 and C_7 are constants.

The displacement is obtained by integrating the velocity, displacement equations (18) are expressed as

$$s=\begin{cases} At^2/2+C_1t+d_1+A\cos(\omega_1 t)/\omega_1^2 & 0<t<t_1 \\ At^2+C_2t+d_2 & t_1<t<t_2 \\ At^2/2+C_3t+d_3-A\cos(\omega_2(t-t_2))/\omega_2^2 & t_2<t<t_3 \\ C_4t+d_4 & t_3<t<t_4 \\ -At^2/2+C_5t+d_5-A\cos(\omega_3(t-t_4))/\omega_3^2 & t_4<t<t_5 \\ -At^2+C_6t+d_6 & t_5<t<t_6 \\ -At^2/2+C_7t+d_7+A\cos(\omega_4(t-t_6))/\omega_4^2 & t_6<t<t_7 \end{cases} \tag{18}$$

where d_1, d_2, d_3, d_4, d_5, d_6 and d_7 are constants.

The proposed method combining quadratic function with cosine is selected to meet processing tasks and applied to trajectories in Y-axis and Z-axis. Based on the requirements of trajectories, the relationship between parameters in Y-axis and Z-axis can be are expressed as

$$\begin{cases} a_{1Z}(0)=0 \quad v_{1Z}(0)=0 \quad s_{1Z}(0)=0 \\ a_{1Z}(t_{11}+t_{22})=0 \quad v_{1Z}(t_{11}+t_{22})=0 \quad s_{1Z}(t_{11}+t_{22})=s_1 \\ a_{1Y}(t_{11})=0 \quad v_{1Y}(t_{11})=0 \quad s_{1Y}(t_{11})=0 \\ a_{3Y}(t_{11}+t_{22}+t_{33})=0 \quad v_{3Y}(t_{11}+t_{22}+t_{33})=0 \\ a_{1Z}(t_{11}+t_{22})=a_{3X}(t_{11}+t_{22}) \\ s_{3Y}(t_{11}+t_{22}+t_{33})=s_3+s_2 \end{cases} \tag{19}$$

The velocity and acceleration can be determined by the given time and displacement in equations (19).

4.1.2 A 3-4-5 polynomial trajectory planning method for operating space

Position, velocity and acceleration of 3-4-5 polynomial motion law can be expressed as

$$\begin{cases} s(t)=a_{max}C_8T^2(C_9\tau^3+C_{10}\tau^4+C_{11}\tau^5) \\ v(t)=a_{max}C_8T(3C_9\tau^2+4C_{10}\tau^3+5C_{11}\tau^4) \\ a(t)=a_{max}C_8(6C_9\tau+12C_{10}\tau^2+20C_{11}\tau^3) \end{cases} \tag{20}$$

where $s(t)$, $v(t)$, and $a(t)$ are position, velocity and acceleration, respectively. C_8, C_9, C_{10} and C_{11} are constants. $a_{max}=S/T^2$, S is the total displacement of motion section, T is the total time of motion. $\tau=t/T$, τ is equivalent to the time operator at the current moment.

4.2 Simulation and analysis

The kinematics model of the RAPMs was established in Matlab. The proposed method and the 3-4-5 polynomial method are used to trajectory planning in operation space. When set the basic parameters s_1=400mm, s_2=100mm, s_3=50mm, t_{00}=0, t_{11}=6.83 s, t_{22}=3.65, t_{33}=4.05 s, t_{44}=10.48 s. The end trajectory can be obtained from Figure 21.

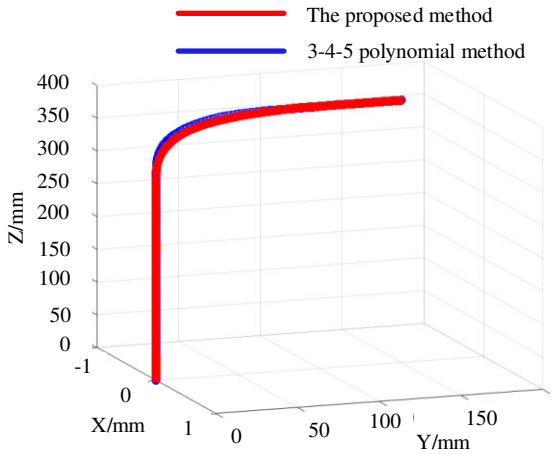

Figure 21 Motion trajectory of the RAPMs

Through analysis of the two trajectories in Figure 21, it is known that motion trajectories of the RAPMs are similar. Compared the proposed method with 3-4-5 polynomial motion law, two methods can pass through key points of the path. The proposed method can make the RAPMs more smooth and steadier corners in movement.

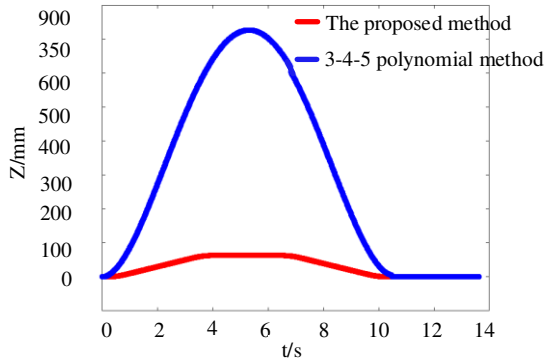

Figure 22 The velocity of motion trajectory of the RAPMs in Z-axis

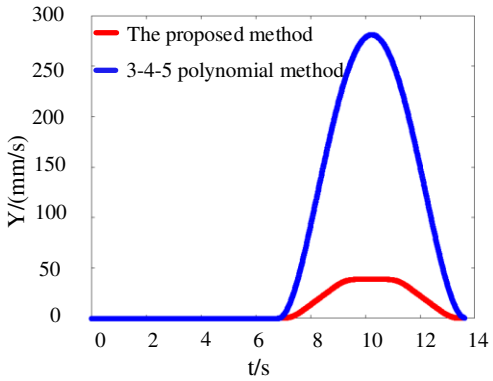

Figure 23 The velocity of motion trajectory of the RAPMs in Y-axis

Through analysis of the velocity of motion trajectory of the RAPMs in Figure 22 and Figure 23, it is known that velocities of the proposed method and 3-4-5 polynomial motion law are continuous and no mutation. The velocity of 3-4-5 polynomial motion law in Y-axis and Z-axis is bigger than the velocity of the proposed method at the same displacement and time. Compared with the 3-4-5 polynomial motion law, the proposed method with amplitude has more adjustable advantages.

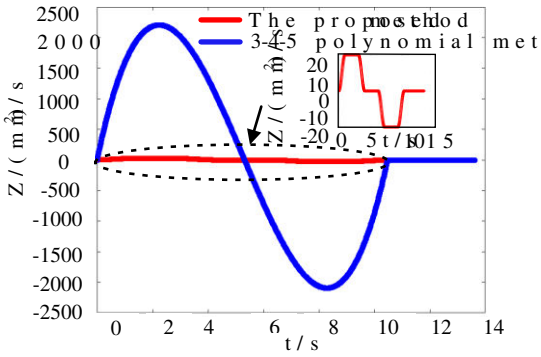

Figure 24 The acceleration of motion trajectory of the RAPMs in the Z direction

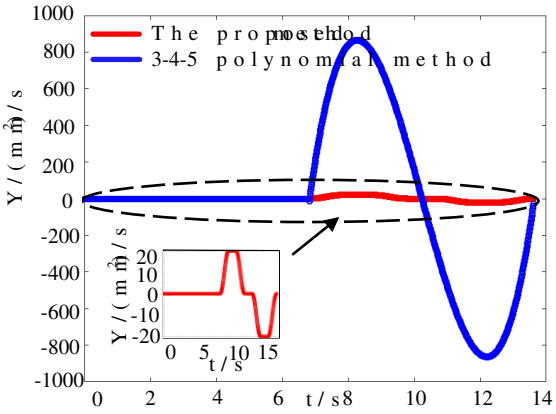

Figure 25 The acceleration of motion trajectory of the RAPMs in the Y direction

Through analysis of the acceleration of motion trajectory of the RAPMs in Figure 24 and Figure 25, it is known that accelerated velocities of the proposed method and 3-4-5 polynomial motion law are also continuous and no mutation. The acceleration of 3-4-5 polynomial motion law in Y-axis and Z-axis is bigger than the acceleration of the proposed method at the same displacement and time. The 3-4-5 polynomial motion law and the proposed method can achieve smooth trajectories. Compared with the 3-4-5 polynomial motion law, the proposed method has lower order and is easier to achieve motion trajectory.

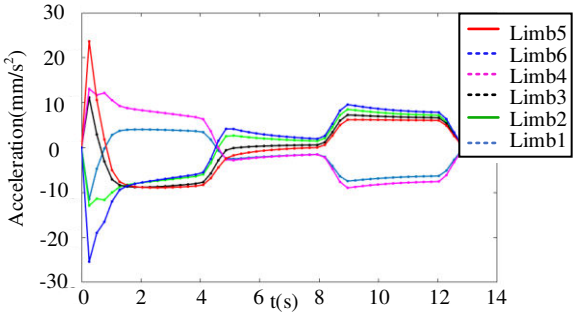

Figure 26 The theoretical acceleration of P actuated joint of limb1

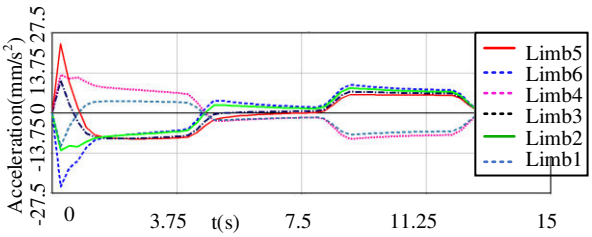

Figure 27 The simulated acceleration of P actuated joint of six limbs

To make the RAPM without vibration impact, the proposed method is applied to motion trajectory of the moving platform of the RAPMs. The theoretical acceleration of P actuated joint of six limbs are obtained in Matlab, as shown in Figure 26. The simulated acceleration

of P actuated joint of six limbs are obtained in Adams, as shown in Figure 27. The dynamic model of the RAPM is shown to be correct by Matlab and Adams based on the proposed method . The acceleration is a continuous curve, the acceleration of six limbs of the RAPM is zero at starting period and ending period. The acceleration increases slowly at starting period of the motion, the acceleration also decays slowly at ending period of the motion, and effectively reduces the RAPM vibration impact, The acceleration of P actuated joint of six limbs is smooth and has no mutation. The proposed method ensures the RAPM in a steady and no impact state.

5 Conclusion

This paper focuses on type synthesis of 5-DOF redundantly actuated parallel mechanisms(RAPMs) for super-large components. A class of the RAPMs with large output rotational angle is synthesized by designing the articulated moving platform and the limbs based on Lie group theory and configuration evolution. Combining Lie group theory with configuration evolution is an intuitive and effective method for synthesizing the RAPMs, the RAPMs can reach $\pm 90^{o}$ by analyzing kinematics of the RAPM. Through analyzing and realizing the motion trajectory of the RAPM, a proposed method of combining quadratic function with the cosine curve is put forward. The proposed method ensures that the RAPM is in the steady-state and have no mechanism impact in the process of motion simulation, the proposed method has lower order and is easier to achieve motion trajectory.

6 Declaration

Acknowledgements

The authors sincerely thanks to Professor Hai-Rong Fang of Beijing Jiaotong University for his critical discussion and reading during manuscript preparation.

Funding

Supported by the Fundamental Research Funds for the Central Universities (No.2018JBZ007)

Availability of data and materials

The datasets supporting the conclusions of this article are included within the article.

Authors' contributions

The author' contributions are as follows: Hai-Rong Fang and Yue-Fa Fang was in charge of the whole trial; Bing-Shan Jiang wrote the manuscript; Li-Tao He assisted with sampling and laboratory analyses.

Competing interests

The authors declare no competing financial interests.

Consent for publication

Not applicable

Ethics approval and consent to participate

Not applicable

References:

[1] A. Syberfeldt, A. Ng, R. I. John, P. Moorec, Multi-objective evolutionary simulation-optimisation of a real-world manufacturing problem. *Robotics and Computer Integrated Manufacturing*, 2009, 25(6): 926-931.

[2] H. M. Martin, J. H. Burge, Progress in manufacturing the first 8.4m off-axis segment for the Giant Magellan Telescope. *Bioinformatics*. 2008, 24(19): 2157–2164.

[3] W. Fan, L. Zheng, W. Ji, A machining accuracy informed adaptive positioning method for finish machining of assembly interfaces of large-scale aircraft components. *Robotics and Computer Integrated Manufacturing*, 2021, 67 (10): 1-19.

[4] Y. G. Li, H. T. Liu, X. M. Zhao, Design of a 3-DOF PKM module for large structural component machining. *Mechanism and Machine Theory*, 2010, 45 (6) 941-954.

[5] S. Huang, J. M. Schimmels, Geometry based synthesis of planar compliances with redundant mechanisms having five compliant components. *Mechanism and Machine Theory*, 2019, 134: 645-666.

[6] L. Wu, C. Dong, G. Wang, An approach to predict lower-order dynamic behaviors of a 5-DOF hybrid robot using a minimum set of generalized coordinates. *Robotics and Computer Integrated Manufacturing*. 2021, 67: 1-12.

[7] B. Lian, T. Sun. Stiffness analysis and experiment of a novel 5-DoF parallel kinematic machine considering gravitational effects. *Robotics and Computer Integrated Manufacturing*, 2015, 95: 82-96.

[8] T. Sun, S. Yang. T. Huang. A finite and instantaneous screw based approach for topology design and kinematic analysis of 5 axis parallel kinematic machines. *Chinese Journal of Mechanical Engineering*, 2018, 31(02): 66-75.

[9] T. Sun, X. Huo. Type synthesis of 1T2R parallel mechanisms with parasitic motions. *Mechanism and Machine Theory*, 2018, 128: 412-428.

[10] J. Yao, W. Guo, Z. Feng, Dynamic analysis and driving force optimization of a 5-DOF parallel manipulator with redundant actuation. *Robotics and Computer Integrated Manufacturing*, 2017, 48): 51-58.

[11] X. Liu, Y. Xu, J. Yao, Control-faced dynamics with deformation compatibility for a 5-DOF active over-constrained spatial parallel manipulator 6PUS-UPU. *Mechatronics*, 2015, 30: 107-115.

[12] L. Kang, W. Kim, B. J. Yi. Modeling and applications of a family of five-degree-of-freedom parallel mechanisms with kinematic and actuation redundancy. *Journal of Mechanisms and Robotics*, 2018, 10(5): 1-16.

[13] S. Krut, S. Rangsri, F. Pierrot, A new 5 degree of freedom redundant parallel mechanism with high tilting capabilities. I*ntelligent Robots and Systems*, 2003, 4(): 3575-3580.

[14] B. Lian, T. Song, Y. Song, Parameter sensitivity analysis of a 5-DoF parallel manipulator. *Robotics and Computer Integrated Manufacturing*, 2017, 46: 1-14.

[15] O. Piccin, B. Bayle, B. Maurin, M. de Mathelin, Kinematic modeling of a 5-DOF parallel mechanism for semi-spherical workspace. *Mechanism and Machine Theory*, 2009, 44(8): 1485-1496.

[16] M. T. Masouleh, C. Gosselin, M. H. Saadatzi, Forward kinematic problem and constant orientation workspace of 5-RPRRR (3T2R) parallel mechanisms. *IEEE. Electrical Engineering*. 2004, 978: 4244-6760.

[17] M. T. Masouleh, C. Gosselin, M. H. Saadatzi, Kinematic analysis of

5-RPUR (3T2R) parallel mechanisms. *Meccanica*, 2011, 46(1): 131-146.

[18] M. T Masouleh, C. Gosselin, Forward kinematic problem of 5-RPUR parallel mechanisms (3T2R) with identical limb structures. *Mechanism and Machine Theory*, 2011, 46(7): 945-959.

[19] M. H. Saadatzi, M. T. Masouleh, H. D. Taghirad. Workspace analysis of 5-PRUR parallel mechanisms (3T2R). *Robotics and Computer Integrated Manufacturing*, 2012, 28: 437-448.

[20] F. Xie, X. Liu, J. Wang, Kinematic optimization of a five degrees-of-freedom spatial parallel mechanism with large orientational workspace. *Journal of Mechanisms and Robotics*, 2017, 9(5): 1-8.

[21] S. Viboon, K. Chooprasird, Dynamics and control of a 5-DOF manipulator based on an H-4 parallel mechanism. *International Journal of Advanced manufacturing technology*, 2011, 52(1-4): 343-364.

[22] H. Ding, W. Cao, C. Cai, Computer-aided structural synthesis of 5-DOF parallel mechanisms and the establishment of kinematic structure databases. *Mechanism and Machine Theory*, 2015, 83 14-30.

[23] P. Wang, X. Wang, Z. Wang, Topology design and kinematic optimization of cyclical 5-DoF parallel manipulator with proper constrained limb, *Advanced Robotics*, 2017, 31(4): 204-219.

[24] Q. Li, Z. Huang, Type synthesis of 3R2T 5-DOF parallel mechanisms using the Lie group of displacements. *IEEE transactions on robotics and automation*, 2004, 20(2): 173-178.

[25] J.M. Hérve, The Lie group of rigid body displacements, a fundamental tool for mechanism design, *Mechanism and Machine Theory*, 1999, 34(5): 719–730.

[26] C. Wang, Y. Fang, H. Fang, Novel 2R3T and 2R2T parallel mechanisms with high rotational capability. *Robotica*, 2017, 35(2): 401-418.

[27] X. Jin, Y. Fang, H. Qu, A class of novel 2T2R and 3T2R parallel mechanisms with large decoupled output rotational angles. *Mechanism and Machine Theory* , 2017, 114: 156-169.

[28] C. Fan, H. Liu Y. Zhang, Type synthesis of 2T2R, 1T2R and 2R parallel mechanisms. *Mechanism and Machine Theory*, 2013, 61: 184-190.

[29] T. Su, H. Zhang, Y. Wang, Trajectory planning for a delta robot based on PH curve. *Robot*, 2018, 40: 45-55.

[30] Z. Wang, X. Zeng, S. Liu, Trajectory planning method for a 2-DOF high-speed parallel manipulator. *International Conference on Intelligent Robotics and Applications*, 2016, 49: 687-694.

[31] J. Jahanpour, M. Motallebi, M. Porghoveh, A novel trajectory planning scheme for parallel machining robots enhanced with NURBS Curves. *Journal of Intelligent & Robotic Systems*, 2016, 82(2): 257-275

[32] D. Chen, S. Li, J. Wang, A multi-objective trajectory planning method based on the improved immune clonal selection algorithm. *Robotics and Computer Integrated Manufacturing*, 2019, 59: 431-442.

[33] J. Kim, E. Croft, Online near time-optimal trajectory planning for industrial robots. *Robotics and Computer Integrated Manufacturing*, 2019, 58: 158-171.

[34] Y. Wang, C. Wu, L. Yu, Trajectory planning of a rolling robot of closed five-bow-shaped-bar linkage. *Robotics and Computer Integrated Manufacturing*, 2018, 53: 81-92.

[35] X. Jiang, E. Barnett, C. Gosselin, Dynamic point to point trajectory planning beyond the static workspace for six-DOF cable suspended parallel robots. *IEEE Transactions on Robotics*, 2018, 34(3): 781-793..

[36] Ü. Dinçer, M. Çevik, Improved trajectory planning of an industrial parallel mechanism by a composite polynomial consisting of Bézier curves and cubic polynomials. *Mechanism and Machine Theory*, 2019, 132: 248-293.

[37] M. Wu, J. Mei, Y. Zhao, Vibration reduction of delta robot based on trajectory planning. *Mechanism and Machine Theory*, 2020, 153 1-15.

[38] D. Reveles R, J. AlfonsoPamanes G, P. Wenger, Trajectory planning of kinematically redundant parallel manipulators by using multiple working modes. *Mechanism and Machine Theory*, 2016, 98 216-230.

[39] H. Wang, W. Heng, J. Huang, Smooth point to point trajectory planning for industrial robots with kinematical constraints based on high order polynomial curve. *Mechanism and Machine Theory*, 2019, 139: 284-293.